

Application of an ARROW model for designing tunable photonic devices

Natalia M. Litchinitser

*OFS Laboratories
25 Schoolhouse Rd., Somerset, NJ 08873, USA
natashal@ofsoptics.com*

Steven C. Dunn

*OFS Specialty Photonics Division
25 Schoolhouse Rd., Somerset, NJ 08873, USA*

**Paul E. Steinvurzel, Benjamin J. Eggleton,
Thomas P. White, Ross C. McPhedran, C. Martijn de Sterke**

*ARC Centre of Excellence for Ultrahigh-bandwidth Devices for Optical
Systems (CUDOS)
School of Physics, University of Sydney, NSW 2006 Australia*

Abstract: Microstructured optical fibers with the low refractive index core surrounded by high refractive index cylindrical inclusions reveal several intriguing properties. Firstly, there is a guiding regime in which the fibers' confinement loss is strongly dependent of wavelength. In this regime, the positions of loss maxima are largely determined by the individual properties of high index inclusions rather than their position and number. Secondly, the spectra of these fibers can be tuned by changing the refractive index of the inclusions. In this paper we review transmission properties of these fibers and discuss their potential applications for designing tunable photonic devices.

©2004 Optical Society of America

OCIS codes: (230.3990) Microstructure devices; (230.7370) Waveguides; (050.2230) Fabry-Perot

References and links

1. V. C. Sundar, A. D. Yablon, J. L. Grazul, M. Ilan, J. Aizenberg, "Fibre-optical features of a glass sponge," *Nature* **424**, 899 - 900 (2003).
2. G. P. Agrawal, *Nonlinear fiber optics* (Academic Press, San Diego, 1995).
3. J. C. Knight, J. Broeng, T. A. Birks, and P. St. J. Russell, "Photonic band gap guidance in optical fibers," *Science* **282**, 1476-1478 (1998).
4. R. F. Cregan, B. J. Mangan, J. C. Knight, T. A. Birks, P. St. J. Russell, P. J. Roberts, D. C. Allan, "Single-mode photonic band gap guidance of light in air," *Science* **285**, 1537-1539 (1999).
5. B. J. Eggleton, C. Kerbage, P. S. Westbrook, R. S. Windeler, and A. Hale, "Microstructured optical fiber devices," *Opt. Express* **9**, 698-713 (2001), <http://www.opticsexpress.org/abstract.cfm?URI=OPEX-9-13-698>.
6. C. M. Smith, N. Venkataraman, M. T. Gallagher, D. Müller, J. A. West, N. F. Borrelli, D. C. Allan, K. W. Koch, "Low-loss hollow-core silica/air photonic bandgap fibre," *Nature* **424**, 657-659 (2003).
7. P. St. J. Russell, "Photonic crystal fibres," *Science* **299**, 358-362 (2003).
8. M. Ibanescu, Y. Fink, S. Fan, E. L. Thomas, J. D. Joannopoulos, "An all-dielectric coaxial waveguide," *Science* **289**, 415-419 (2000).
9. C. Kerbage and B. J. Eggleton, "Tunable microfluidic optical fiber gratings," *Appl. Phys. Lett.* **82**, 1338-1340 (2003).

10. C. Kerbage, P. Steinvurzel, P. Reyes, P. S. Westbrook, R. S. Windeler, A. Hale, B. J. Eggleton, "Highly tunable birefringent microstructured optical fiber," *Opt. Lett.* **27**, 842-844 (2002).
11. M. van Eijkelenborg, M. Large, A. Argyros, J. Zagari, S. Manos, N. A. Issa, I. M. Bassett, S. C. Fleming, R. C. McPhedran, C. M. de Sterke, and N. A. P. Nicorovici, "Microstructured polymer optical fibre," *Opt. Express* **9**, 319-327 (2001), <http://www.opticsexpress.org/abstract.cfm?URI=OPEX-9-7-319>
12. J. C. Knight, "Photonic crystal fibres," *Nature* **424**, 847-851 (2003).
13. R. T. Bise, R. S. Windeler, K. S. Kranz, C. Kerbage, B. J. Eggleton, and D. J. Trevor, "Tunable photonic band gap fiber," in *OSA Trends in Optics and Photonics (TOPS) Vol. 70*, Optical Fiber Communication Conference, Technical Digest, Postconference Edition (Optical Society of America, Washington DC, 2002), pp. 466-468.
14. T. T. Larsen, A. Bjarklev, D. S. Hermann, J. Broeng, "Optical devices based on liquid crystal photonic bandgap fibres," *Opt. Express* **11**, 2589-2596 (2003).
15. N. M. Litchinitser, A. K. Abeeluck, C. Headley, B. J. Eggleton, "Antiresonant reflecting photonic crystal optical waveguides," *Opt. Lett.* **27**, 1592-1594(2002).
16. A. K. Abeeluck, N. M. Litchinitser, C. Headley, B. J. Eggleton, "Analysis of spectral characteristics of photonic bandgap waveguides," *Opt. Express* **10**, 1320-1333 (2002), <http://www.opticsexpress.org/abstract.cfm?URI=OPEX-10-23-1320>
17. T. P. White, R. C. McPhedran, C. Martijn de Sterke, N. M. Litchinitser, B. J. Eggleton, "Resonance and scattering in microstructured optical fibers," *Opt. Lett.* **27**, 1977-1979 (2002).
18. N. M. Litchinitser, S. C. Dunn, B. Usner, B. J. Eggleton, T.P. White, R.C. McPhedran, C. Martijn de Sterke, "Resonances and modal cutoff in microstructured optical waveguides," *Opt. Express* **11**, 1243-1251 (2003), <http://www.opticsexpress.org/abstract.cfm?URI=OPEX-11-10-1243>
19. M. A. Duguay, Y. Kukubun, T. L. Koch, L. Pfeiffer, "Antiresonant reflecting optical waveguides in SiO₂-Si multiplayer structures," *Appl. Phys. Lett.* **49**, 13-15 (1986).
20. A. Iocco, H. G. Limberger, R. P. Salathé, L. A. Everall, K. E. Chisholm, J. A. R. Williams, I. Bennion, "Bragg grating fast tunable filter for wavelength division multiplexing," *J. Lightwave Technol.* **17**, 1217-1221 (1999).
21. H. Y. Liu, G. D. Peng, P. L. Chu, "Polymer fiber Bragg gratings with 28 dB transmission rejection," *IEEE Photon. Technol. Lett.* **14**, 935-937 (2002).
22. R. Scarmozzino, A. Gopinath, R. Pregla, S. Helfert, "Numerical techniques for modeling guided-wave photonic devices," *IEEE J. Select. Topics Quantum Electron.* **6**, 150-162 (2000).
23. T. P. White, B. T. Kuhlmeier, R. C. McPhedran, D. Maystre, G. Renversez, C. Martijn de Sterke, L. C. Botten, "Multipole method for microstructured optical fibers. I. Formulation," *J. Opt. Soc. Am. B* **19**, 2322-2330 (2002).
24. B. T. Kuhlmeier, T. P. White, G. Renversez, D. Maystre, L. C. Botten, C. Martijn de Sterke, R. C. McPhedran, "Multipole method for microstructured optical fibers. II. Implementation and results," *J. Opt. Soc. Am. B* **19**, 2331-2340 (2002).
25. H. C. van de Hulst, *Light Scattering by Small Particles* (Wiley, New York, 1957).
26. A. C. Lind and J. M. Greenberg, "Electromagnetic scattering by obliquely oriented cylinders," *J. Appl. Phys.* **37**, 3195-3203 (1966).
27. A. W. Snyder and J. D. Love, *Optical waveguide theory* (Chapman and Hall, New York, 1983)

1. Introduction

Optical fibers, which are essentially dielectric structures transmitting electromagnetic waves at optical frequencies, exist in a large variety of forms. They can be natural such as the glass sponge [1] as well as artificially made [2]. Their applications range from long-haul telecommunications to medicine, spectroscopy and sensors. Recently, a new class of optical fibers, microstructured optical fibers (MOFs) or photonic crystal fibers, has been introduced [3-12]. These fibers are made of glass or polymer with a cross-section containing a structure on the scale of a micron. The presence of this structure (often in the form of circular air-holes or concentric cylinders) changes the transmission characteristics of the fiber. Many properties of MOFs are determined by the air-hole size and the spacing between them. Moreover, once the fiber has been made, its properties can be further modified by introducing various materials into the air-holes [13,14]. Using materials with variable thermal or electro-optic properties allows the fibers to be reversibly tuned. Additional degrees of design

freedom provided by MOFs are being utilized in various photonic devices including microfluidic fiber gratings [9] or dynamically tunable MOFs [10].

MOFs with a solid core surrounded by air-holes guide light through a modified total internal reflection (TIR) mechanism. Filling the air-holes with high-index material rules out TIR-based guidance, since the refractive index of the core is lower than that of the cladding. Recently, the guiding properties of MOFs consisting of a low refractive index core and air-holes filled with high refractive index material [15-18] were investigated. A spectral response of these fibers is approximately periodic in frequency. A new guiding regime was identified in which the positions of spectral minima are largely determined by the individual properties of high index inclusions rather than their position and number. The physical mechanism of guiding in this regime is similar to that in antiresonant reflecting optical waveguides (ARROW) [19], widely used in the field of integrated optics. A simple analytical model was proposed to predict the locations of spectral minima based on the geometry and refractive indexes of the inclusions.

In a present paper we show how this simple model can be used for manipulating the properties of MOF with high-index inclusions and designing tunable fiber devices. A large variety of tunable photonic devices has been described in the literature including silica fiber-Bragg-grating-based (FBG) filters [20], polymer Bragg gratings [21], tunable filters based on

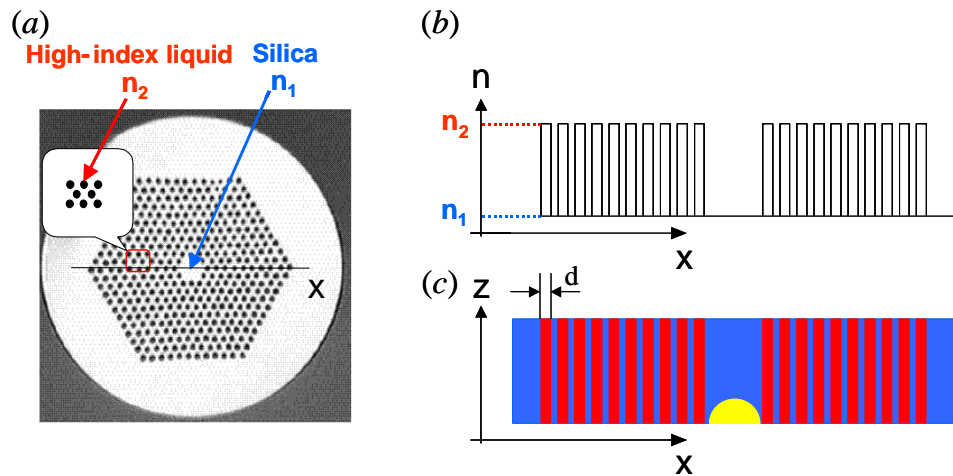


Fig. 1. (a) MOF with low-index core and high-index inclusions, (b) Corresponding cross-section of the refractive index profile along x axis, (c) Planar optical waveguide with low-index core and high-index layers.

FBG and long-period gratings (LPGs) written in an index-guiding MOF [9,10]. A majority of the filtering applications requires introducing some kind of a resonant structure inside the core of the fiber such as FBGs or LPGs. Once such a resonant structure is introduced, its properties can be tuned only within a certain wavelength range that is determined by the properties of the fiber material (silica or polymer). ARROW-like MOFs with high index inclusions have several advantages for designing tunable devices. First, their spectral response consists of many narrow resonant features that are approximately periodically spaced in frequency. Therefore, no additional resonant structures are required to be introduced. The positions of these resonances are largely determined by the refractive indexes of the inclusions and the background material (silica or polymer), and by the size of the high-index inclusion. Second, ARROW-like MOFs offer a possibility of a more flexible tuning range compared to grating-based devices, which could be achieved by replacing the high-index material in the

air-holes. A simple analytical model reviewed here takes into account advanced features of ARROW-like MOFs and thus could be utilized in designing of tunable photonic devices.

In the following sections we review a theory that allows prediction of the transmission spectrum minima in MOF with high index inclusions (Section II) and discuss the possibility of designing novel photonic devices utilizing MOF with tunable refractive index of the cylindrical inclusions (Section III). Our findings are summarized in Section IV.

2. Theory

2.1 Planar waveguide: Antiresonant reflecting optical waveguide mode

The cross-section of a typical MOF consisting of a low-index solid core surrounded by ten hexagonal rings of circular air-holes filled with high-index liquid is shown in Fig. 1(a). The refractive index profile of this fiber along x direction is given in Fig. 1(b). Initially we simplify MOF by reducing it to a one-dimensional planar waveguide having a similar refractive index profile as shown in Fig. 1(c) [16]. The propagation of a Gaussian beam in z direction has been investigated using the standard beam propagation method (BPM)[22]. The transmission spectrum is defined as the ratio of the integrated power within the core region at the end of the waveguide to that launched into the core. The main results of the simulations can be summarized as follows. First, the locations of the spectral minima are essentially unaffected by changes in lattice constant, provided that the refractive indexes (n_1, n_2) and the thickness of high-index layer d were kept constant. Second, the locations of the spectral minima remain unchanged when all layers except one on each side of the core were removed. Finally, the transmission minima shifted in either of the following cases: (i) d was changed while n_1 and n_2 were kept constant, or (ii) d was kept constant, while n_1 or n_2 were changed. These simulations identified a guiding regime in which the properties of high-index layer largely determine the spectral properties of the entire waveguide. In this regime the addition of new layers and changing their spacing results in a better confinement and an appearance of some fine structure near the transmission minima (that becomes increasingly more noticeable at longer wavelengths, see Ref. [16]). These conclusions allow us to simplify the problem by replacing a 10-layer structure in Fig. 1(b) by 1-layer structure shown in Fig. 2(a). Figure 2(b) shows the calculated spectrum for $n_1=1.4$, $n_2=1.8$, $d=3.437\mu\text{m}$ and a waveguide length of 5cm. Electric field profiles at wavelengths corresponding to (1) a high transmission at $\lambda=0.676\mu\text{m}$, and (2) a transmission minimum at $\lambda=0.707\mu\text{m}$ are shown in Fig. 2(c). The electric field oscillations inside the high-index layer are enlarged in Fig. 2(d). It is noteworthy that at wavelengths corresponding to transmission minima, the electric field forms a standing wave pattern with an integer number of half-oscillations inside the high-index layer. This suggests that the guiding mechanism in this type of waveguides is very similar to an antiresonant reflecting optical waveguide (ARROW) principle [19]. In ARROW light is confined in the core by antiresonant reflection from the high-index layers in the cladding. Each high-index layer can be considered as a Fabry-Perot-like (FP) resonator. Narrow-band resonances of this FP resonator correspond to transmission minima for the light propagating in the core. Therefore, at resonance the high-index layer becomes effectively transparent and light escapes completely from the entire structure. Wide antiresonances of the FP correspond to high transmission regions.

The resonant condition for a high-index layer is given by $k_t d = \pi m$, where $k_t = \frac{2\pi}{\lambda} \sqrt{n_2^2 - n_1^2}$. We assume that light impinges the core/cladding interface at glancing angles (i.e. $\lambda a \ll 1$). The wavelengths corresponding to transmission minima are given by:

$$\lambda_m = \frac{2d}{m} \sqrt{n_2^2 - n_1^2}, \text{ where } m = 1, 2, \dots \quad (1)$$

Obviously, the simple model described here is valid only in a “short wavelength” regime defined by $\lambda/d \leq 2\sqrt{n_2^2 - n_1^2}$.

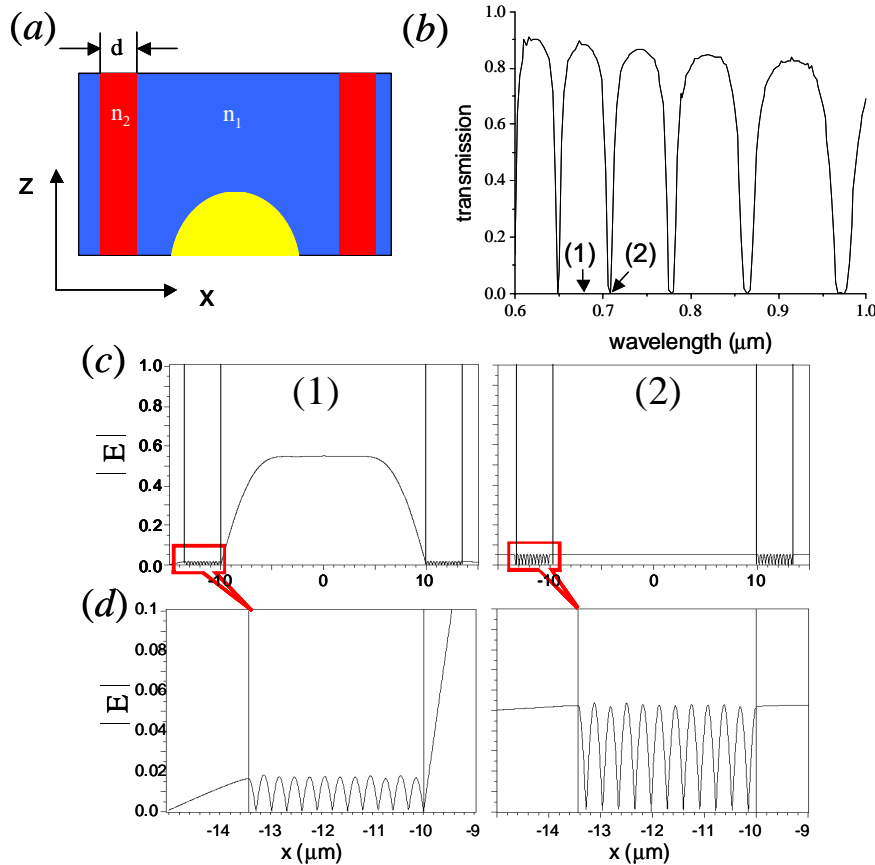


Fig. 2. (a) A schematic of a waveguide, (b) Corresponding transmission spectrum at a distance of 5cm in z direction, (c) Electric field profile at a distance of 5cm at the wavelength corresponding to high transmission (1) and a transmission minimum (2), (d) Electric field oscillations inside the high-index layer.

2.2 Microstructured fiber: Scattering resonances

In this section we study the possibility of extending the ARROW model to understand the mechanism for light propagation in MOFs with high-index inclusions embedded in a low-index background, as shown in Fig. 1. In Ref. [17] using a rigorous multipole method [23,24] we numerically calculated the complex propagation constant β (and the corresponding effective refractive index) of the fundamental mode for various MOF configurations including a three-ring hexagonal structure, a single hexagonal ring structure, a ten-cylinder-ring structure and even ten cylinders arranged randomly around the core. The modal effective refractive index n_{eff} in these structures always contains a real and an imaginary part since the structures are leaky. The imaginary part of n_{eff} is proportional to the confinement loss. The results of these simulation can be summarized as follows: although the actual values of the effective refractive index and loss vary for each of the above structures, the shapes of the loss curves are similar and the high-loss regions occur near the same wavelengths for all fiber configurations. The only parameters that were kept constant in all cases were the cylinder

diameter $d=3.315\mu\text{m}$, low refractive index $n_1=1.44$ (background) and high refractive index $n_2=1.8$ (inside the cylinders). This suggested that the properties of individual high-index cylinders largely determine the locations of high-loss regions.

This notion was confirmed by studying the scattering of a plane wave at oblique incidence upon the surface of an infinite cylinder (shown in Fig. 3(a)) [25,26]. The scattering properties can be characterized by a scattering cross section and a forward-to-backward scattering ratio which is a measure of the ratio of the energy flowing out of the cylinder to the energy reflected back. Figure 3(b) shows good qualitative agreement between MOF confinement loss and forward-to-backward scattering ratio for a plane wave scattered on a single high-index cylinder. The angle of incidence of the plane wave was varied according to the effective index of the MOF mode at each wavelength.

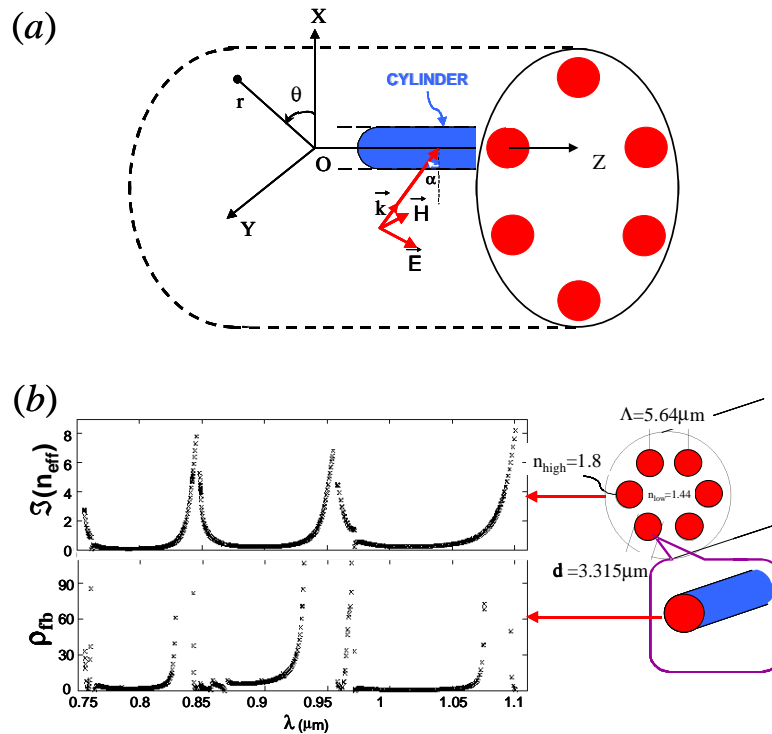


Fig. 3 Comparison of MOF loss properties with forward-to-backward scattering ratio for the plane wave scattering on a single cylinder.

These results indicate that the modal loss properties of MOFs with high-index inclusions surrounding a low-index cladding can be understood in terms of a plane wave scattering from a single cylinder and are therefore determined by the properties of individual cylinders rather than by their positions and number. Next section describes how to predict the locations of the high-loss regions analytically, in a manner similar to the planar waveguide case.

2.3 Modal cutoff

In previous sections a new guidance regime was described in which the positions of loss minima depend on the properties of individual high-index inclusions. Now we consider each high-index inclusion as a step-index waveguide with a high-index core (with the refractive index n_2) and a low-index cladding (with the refractive index n_1). Let's start with a planar waveguide shown in Fig. 1(c) first. The properties of a step-index waveguide are well

understood. At a given wavelength the waveguide supports N guided modes with modal effective refractive indices in the range $n_1 < n_{eff} < n_2$. The effective refractive index of the highest order mode supported is the closest to the refractive index of the cladding. As the wavelength increases, n_{eff} approaches the refractive index of the cladding n_1 . A wavelength at which the waveguide switches from supporting $n+1$ modes to n modes is referred to as modal cutoff wavelength for a particular mode. In a planar waveguide no power of the mode can propagate in the high-index core at cutoff and all the modes' power is in the cladding. Modal group velocity given by [27]

$$v_g = \frac{c}{n_2^2} \frac{\beta}{k} \frac{1}{1-2\Delta(1-\eta)} \quad (2)$$

where c is the speed of light, n_2 is the refractive index of the core, $\Delta = (n_2^2 - n_1^2)/2n_2^2$, η is the fraction of modal power residing in the core. At cutoff $\eta \rightarrow 0$ and, therefore, the modal group velocity approaches the speed of light in the cladding c/n_1 .

Next, we establish a link between the properties of a single high-index inclusion at cutoff and the properties of the entire ARROW structure consisting of a low-index core n_1 and high-index n_2 layers in the cladding (as shown in Fig. 1(c)). The fundamental and other lower order modes of this waveguide impinge the core-cladding interface at glancing angles (assuming $\lambda/a \ll 1$). Therefore the effective refractive index of the core mode is approximately equal to that of the core material n_1 , $n_{eff} = n_1 \cos(\theta) \approx n_1$. As the wavelength approaches that corresponding to the modal cutoff of the high-index inclusion, the effective refractive index of the highest order mode of the inclusion approaches n_1 . Therefore at the cutoff wavelength of the high-index layer mode, the effective refractive index of the entire structure approaches n_1 as shown in Fig. 4. Upper plot in Fig. 4 shows the effective refractive index of the modes of the high-index layer. Lower plot corresponds to the effective refractive index of the low-index core mode of the entire ARROW structure. At a cutoff wavelength the entire waveguide structure becomes effectively transparent. Therefore, in order to find the wavelengths corresponding to the high loss regions for the entire ARROW structure, one needs to find modal cutoff conditions for the modes of a single high-index inclusion (layer or cylinder). For the planar structure this condition is equivalent to the resonant condition for the high-index layer given by Eq. (1). The modal properties of planar and cylindrical waveguide modes are not the same at the cutoff condition. Only some of the modes of the cylindrical step-index waveguide have zero power within the core at cutoff [27]. These include the TE_{0m} , TM_{0m} , HE_{1m} and HE_{2m} modes. Therefore, according to the Eq. (2) only these modes have a group velocity equal to the speed of light in the cladding c/n_1 (and $n_{eff} = n_1$). All other modes have some fraction of their power propagating in the core with the velocity smaller than c/n_1 (and $n_{eff} > n_1$). It seems reasonable that since only specific modes of the high-index inclusions have $n_{eff} = n_1$ at the cutoff, only those modes lead to appearance of the transmission minima of the entire structure. Therefore, in order to predict spectral minima of the entire MOF one needs to find modal cutoff wavelengths for TE_{0m} , TM_{0m} , HE_{1m} and HE_{2m} modes.

For TE_{0m} and TM_{0m} modal cutoff condition is given by [27]

$$J_0(k_t d/2) = 0. \quad (3)$$

For HE_{1m} mode modal cutoff is given by

$$J_1(k_t d/2) = 0. \quad (4)$$

Resonance conditions for $k_t d/2$ can be found analytically using the cosine approximation for the Bessel functions J_ν when $k_t d/2 \gg \nu$.

From Eqs. (3) and (4) resonant wavelengths can be written as follows:

$$\lambda_m = \frac{2d\sqrt{n_2^2 - n_1^2}}{m+1/2}, \quad m = 1, 2, \dots \quad (5)$$

For HE_{2m} the cutoff condition is given by

$$\frac{k_t d J_0(k_t d/2)}{2 J_1(k_t d/2)} = \frac{2\Delta}{1-2\Delta} \quad (6)$$

The solution of transcendental Eq. (6) is very close to the solution of Eq. (3) given by Eq. (5) as long as

$$\frac{4\Delta}{1-2\Delta} \frac{1}{k_t d} \ll 1. \quad (7)$$

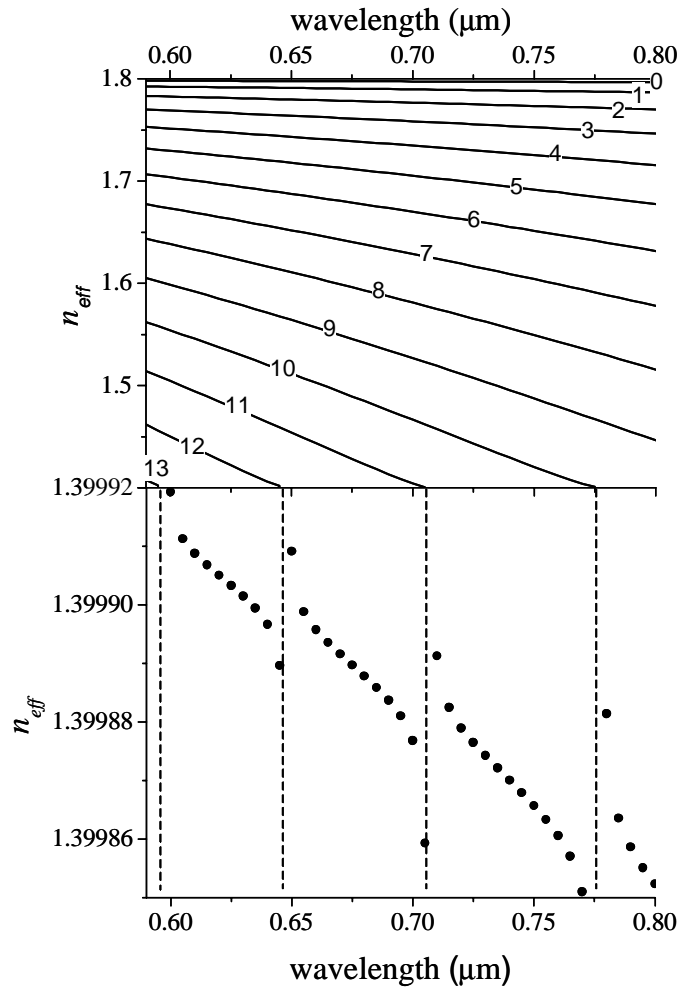


Fig. 4. Upper plot shows the effective refractive index of the modes of the high-index layer as a function of the wavelength. Lower plot shows the effective refractive index of the mode propagating in the low-index core of the entire ARROW structure. Vertical dashed lines correspond to the modal cutoffs.

In our numerical example (shown in Fig. 3) $\frac{4\Delta}{1-2\Delta} \frac{1}{k_i d} = 0.037 \pm 0.055$. Therefore the condition (5) can be used to predict the high-loss spectral wavelengths in wide range of parameters. The analytical predictions of equation (5) are compared to numerical results obtained using the multipole method [18].

While closed-form analytical solutions for modal cutoff can be found in a limited number of cases such as a step-index planar or cylindrical waveguide, we can always find the cutoff wavelengths for other geometries of the high index inclusions numerically. Therefore, using the present approach spectral minima of any microstructured waveguide with low index core and high index inclusions of various shapes can be found, as long as these inclusions form waveguides.

In summary, it has been shown that the positions of spectral minima can be determined by calculating the modal cutoff wavelength of the high-index regions, and thus they depend only on the mode structure of those inclusions. Equations (1) and (5) provide good predictions for the positions of transmission minima (confinement loss maxima). Therefore, the complex problem of analyzing the properties of microstructured optical waveguides can be reduced to the much simpler problem of analyzing the modal cutoff properties of an individual high-index inclusion.

3. Potential applications

As shown in Fig. 2, the spectrum of an ARROW waveguide consists of several narrow transmission dips at wavelengths λ_m . These spectral dips can be utilized for making tunable optical filters. Since the resonant wavelengths in Eqs. (1) and (5) are functions of n_2 , the position of the spectral dips can be shifted by changing n_2 . Experimentally this can be realized by using materials with temperature dependent refractive index [13,14].

Resonant wavelength shift in planar and cylindrical geometries is given by

$$\Delta\lambda_m = 2d \left(\sqrt{n_2^2(T_2) - n_1^2} - \sqrt{n_2^2(T_1) - n_1^2} \right) \left\{ \begin{array}{l} m^{-1} \\ (m+1/2)^{-1} \end{array} \right. , \quad (8)$$

respectively.

In Eq. (8) we assume that the temperature sensitivity of a high-index material n_2 is much higher than that of the background material n_1 . However, Eq. (8) can be easily modified to include the temperature dependence on n_1 .

Let's consider designing a tunable filter based on ARROW-like planar waveguide or MOF. First we design a continuously tunable filter based on the planar waveguide shown in Fig. 2.

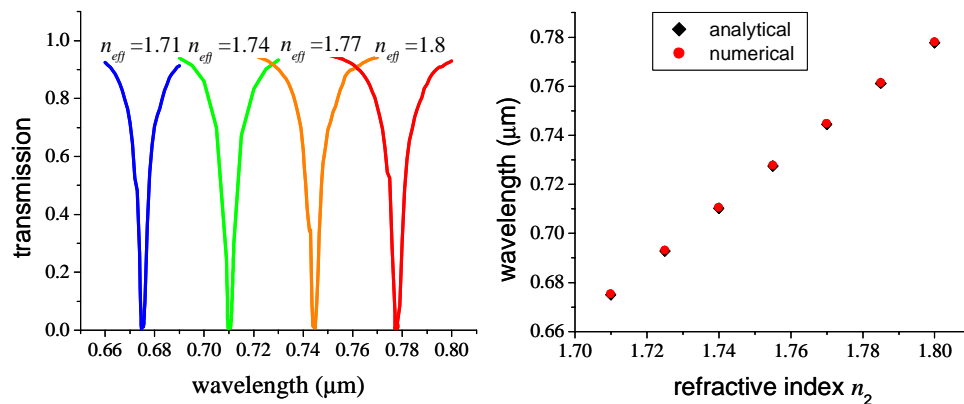


Fig. 5. (a) Transmission minimum ($m=10$) for different values of n_2 , for fixed values of $n_1=1.4$, $d=3.437\mu\text{m}$. (b) Comparison of the analytical predictions and the numerical simulations for the location of the transmission minimum.

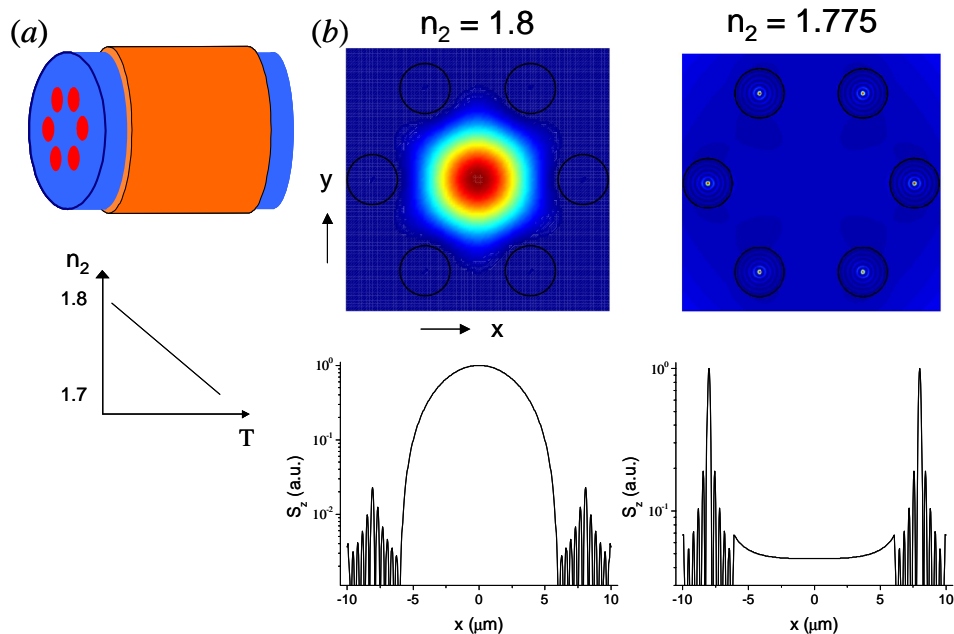


Fig. 6. (a) Schematic of MOF with a micro-heater. MOF air-holes are filled with a high-index material whose refractive index n_2 changes with temperature T , (b) Longitudinal component of Poynting vector S_z for the lowest order MOF mode in transmission mode ($n = 1.8$) and in filter mode ($n = 1.775$) along with x cross section of S_z .

We choose a particular transmission dip at $\lambda = 0.777 \mu\text{m}$, corresponding to $m = 10$ in Eq. (1). Figure 5(a) shows the evolution of this peak over the wavelength as n_2 decreases. Comparison of the numerical results and analytical predictions for the location of the minimum versus n_2 is shown in Fig. 5(b). Note, that even though ARROW-type of waveguide is inherently lossy, that should not preclude this waveguide from being used as a filter since only a short piece of fiber is required for this application. Alternatively, additional high-index layers can be used to reduce the confinement loss.

A type of filter described here can be realized in MOF geometry by placing a micro-heater on a surface of MOF filled with thermally tunable material such as a high index liquid ($n_{589 \text{ nm}} = 1.8$, Cargille Laboratories series M with a temperature dependence of the refractive index given by $dn/dT = -6.8 \cdot 10^{-4} / \text{deg C}$). The schematic of the device is shown in Fig. 6(a). In this example we use Eq. (5) to find a value for the refractive index n_2 at which the MOF with one ring of high-index inclusions switches from a transmission mode at initial (room) temperature to a filtering mode for $\lambda = 0.7525 \mu\text{m}$ when the temperature increases.

Here we assume that the refractive index n_2 decreases with temperature and equals 1.8 at room temperature. The refractive index required to tune the MOF was found to be 1.775. In this example other fiber parameters are $n_1 = 1.44$, $d = 3.8 \mu\text{m}$, $\Lambda = 8 \mu\text{m}$. Figure 6(b) shows the longitudinal component of the Poynting vector S_z and its cross section along x axis for the lowest-order mode for $n_2(T_1) = 1.8$ and $n_2(T_2) = 1.775$ calculated using the multipole method [23,24]. However, multipole simulations only provide an information about a particular core mode and do not explicitly show where the power goes when it disappears from the core at a resonant wavelength. BPM provides more information about the light propagation and the results obtained from simulations using BPM can be directly compared with experiments.

We used a BPM to propagate a Gaussian beam in z direction in 1mm of ARROW-like MOF with two rings of inclusions shown in Fig. 7(a). A second ring of inclusions has been

added to reduce the power leakage from the core. All other parameters are identical to those in Fig. 6. Figure 7(b) shows the transmission spectra for two cases: $n_2 = 1.8$ (red line) and $n_2 = 1.775$ (black line). Both spectra are taken after beam propagated along the fiber (in z -direction) at $z = 1$ mm. Simulations shown in Fig. 7(c) and 7(d) further illustrate the dynamic of light propagation in ARROW-like MOF at a design wavelength $\lambda = 0.7525 \mu\text{m}$ for $n_2 = 1.8$ (off-resonance) and $n_2 = 1.775$ (on-resonance), respectively. At this wavelength light propagates in the low-index core when $n_2 = 1.8$, since $\lambda = 0.7525 \mu\text{m}$ corresponds to a high transmission part of the spectrum. Animation in Fig. 7(d) clearly shows that light escapes from the entire structure at the same wavelength when $n_2 = 1.775$. These simulations confirm that the MOF switches from a high transmission mode to a filtering mode as the refractive index changes as predicted by Eq. (5).

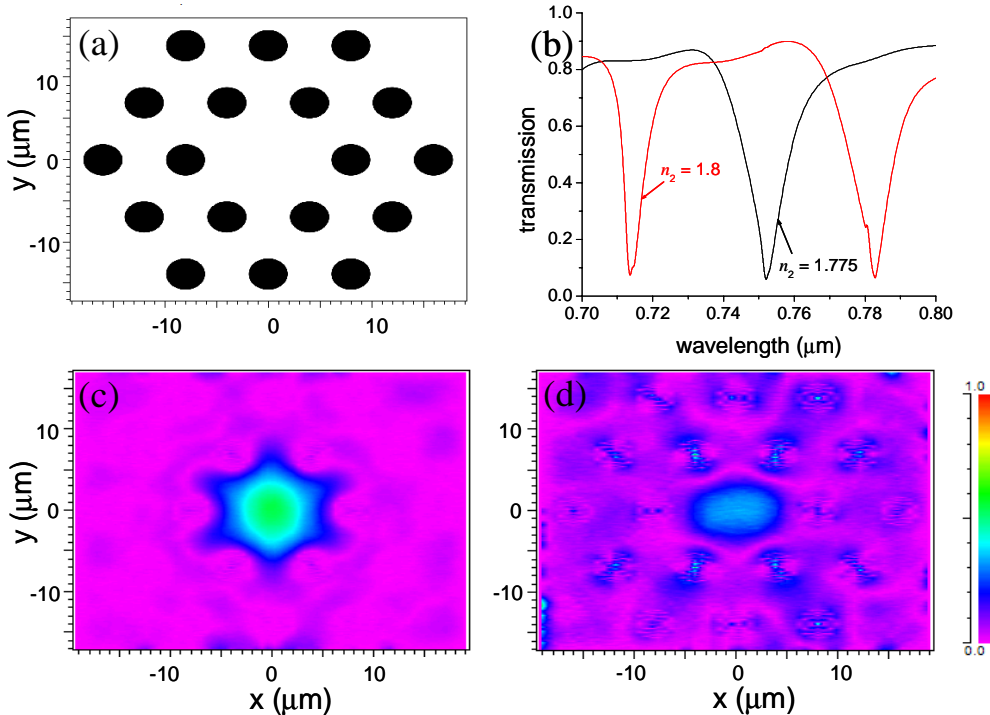


Fig. 7. (a) MOF profile used in BPM simulations, (b) Transmission spectra at $z = 1$ mm, (c) (1446 KB) Evolution of the beam profile in MOF with $n_2 = 1.8$ (the frame shows output beam profile at $z = 1$ mm), (d) (1446 KB) Evolution of the beam profile in MOF with $n_2 = 1.775$ (the frame shows output beam profile at $z = 1$ mm).

4. Summary

We reviewed some simple analytical approaches developed for understanding the spectral properties of MOFs with low refractive index core surrounded by high refractive index inclusions. Using the insight gained from a simple physical picture of light confinement and propagation in these MOFs, we demonstrated how the properties of these fibers can be adjusted in a controlled and predictable way providing a basis for novel photonic devices.

Acknowledgments

This work was produced with the assistance of the Australian Research Council (ARC) under the ARC Centres of Excellence Program. CUDOS (the Centre for Ultra-high bandwidth Devices for Optical Systems) is an ARC Centre of Excellence.